Optical Images of an Exosolar Planet 25 Light Years from Earth*

Paul Kalas[1*], James R. Graham[1], Eugene Chiang[1,2], Michael P. Fitzgerald[3], Mark Clampin[4], Edwin S. Kite[2], Karl Stapelfeldt[6], John Krist[6]

[1]Astronomy Department, University of California,
Berkeley, CA 94720, USA
[2]Department of Earth & Planetary Science, University of California, Berkeley, CA 94720, USA
[3]Institute of Geophysics & Planetary Science, Lawrence Livermore National Laboratory
Livermore, CA 94551, USA
[4]Exoplanets & Stellar Astrophysics Laboratory, Goddard Space Flight Center,
Greenbelt, MD 20771, USA
[6]MS 183-900, Jet Propulsion Laboratory, Caltech, Pasadena, CA 91109, USA

*Accepted for publication in *Science*

Fomalhaut is a bright star 7.7 parsecs (25 light years) from Earth that harbors a belt of cold dust with a structure consistent with gravitational sculpting by an orbiting planet. Here, we present optical observations of an exoplanet candidate, Fomalhaut b. In the plane of the belt, Fomalhaut b lies approximately 119 astronomical units (AU) from the star, and within 18 AU of the dust belt. We detect counterclockwise orbital motion using Hubble Space Telescope observations separated by 1.73 years. Dynamical models of the interaction between the planet and the belt indicate that the planet's mass is at most three times that of Jupiter for the belt to avoid gravitational disruption. The flux detected at 0.8 μm is also consistent with that of a planet with mass no greater than a

few times that of Jupiter. The brightness at 0.6 μm and the lack of detection at longer wavelengths suggest that the detected flux may include starlight reflected off a circumplanetary disk, with dimension comparable to the orbits of the Galilean satellites. We also observed variability of unknown origin at 0.6 μm.

Approximately 15% of nearby stars are surrounded by smaller bodies that produce copious amounts of fine dust via collisional erosion (*1*). These "dusty debris disks" are analogues to our Kuiper Belt, and can be imaged directly through the starlight they reflect or thermal emission from their dust grains. Debris disks may be gravitationally sculpted by more massive objects; their structure gives indirect evidence for the existence of accompanying planets (e.g., *2, 3*). Fomalhaut, an A3V star 7.69 pc from the Sun (*4*), is an excellent example: a planet can explain both the observed 15 AU offset between the star and the geometric center of the belt, and the sharp truncation of the belt's inner edge (*3, 5–7*). With an estimated age of 100–300 Myr (*8*), any planet around Fomalhaut would still be radiating its formation heat, and would be amenable to direct detection. The main observational challenge is that Fomalhaut is one of the brightest stars in the sky (m_V=1.2 mag); to detect a planet around it requires the use of specialized techniques such as coronagraphy to artificially eclipse the star and suppress scattered and diffracted light.

Detection of Fomalhaut b

Coronagraphic observations with the Hubble Space Telescope (HST) in 2004 produced the first optical image of Fomalhaut's dust belt, and detected several faint sources near Fomalhaut (*6*). Fomalhaut's proper motion across the sky is 0.425 arcsecond per year in the southeast direction, which means that objects that are in the background will appear to move northwest

relative to the star. To find common proper motion candidate sources, we observed Fomalhaut using the Keck II 10-m telescope in 2005 and with HST in 2006 (SOM). In May, 2008, a comprehensive data analysis revealed that Fomalhaut b is physically associated with the star and displays orbital motion. Follow-up observations were then conducted at Gemini Observatory at 3.8 μm (SOM).

Fomalhaut b was confirmed as a real astrophysical object in six independent HST observations at two optical wavelengths (0.6 μm and 0.8 μm; see Fig. 1 and Table S1). It is co-moving with Fomalhaut, except for a 0.184 $\pm$ 0.022 arcsecond (1.41 $\pm$ 0.17 AU) offset between 2004 and 2006 (ΔT = 1.73 yr), corresponding to 0.82 $\pm$ 0.10 AU yr^{-1} projected motion relative to Fomalhaut (SOM). If Fomalhaut b has an orbit that is coplanar and nested within the dust belt, then its semimajor axis is $a \simeq 115$ AU (due to the offset geometry, the current stellocentric separation is 119 AU). An object with a = 115 AU in near-circular Keplerian motion around a star with mass 2.0 M$_\odot$ has an orbital period of 872 years, with an average orbital velocity of 0.83 AU yr^{-1}. Our observations are therefore consistent with Keplerian motion.

Fomalhaut b is located near the faint half of the belt seen in stellar light backscattered by dust grains. Therefore it lies behind the sky plane (the Earth-Fomalhaut-Fomalhaut b angle is 126$^{\rm o}$), at approximately 51$^{\rm o}$ past conjunction as it orbits counter-clockwise. Though faint, Fomalhaut b is still one hundred times brighter than reflected light from a Jupiter-like planet at that radius from Fomalhaut (SOM).

Dynamical Models of Planet-Belt Interaction

We constrain the orbit and mass of Fomalhaut b by modeling its gravitational influence on the dust belt, reproducing properties of the belt inferred from the HST scattered light images. Our modeling procedure takes four steps. First, for a given mass and orbit of Fomalhaut b, we create a population of several thousand parent bodies stable to gravitational perturbations from

the planet. These parent bodies, modeled as test particles, do not undergo close encounters with Fomalhaut b over 100 Myr. Initial parent body orbits have semimajor axes between 120 and 140 AU, and eccentricities and longitudes of periastron that are purely secularly forced by the planet (*9*). Initial inclinations of parent bodies are randomly and uniformly distributed within 0.025 radian of Fomalhaut b's orbital plane, and remaining orbital angles are drawn at random. The forced orbits thus constructed are nested ellipses of eccentricity ≈ 0.11 that approximate the observed belt morphology. Forced orbits are expected to result from interparticle collisions, which dissipate random motions and compel planetesimals to conform towards closed, non-intersecting paths (*10*).

This elliptical annulus of parent bodies is termed a "birth ring" (*11*); erosive collisions among parent bodies give birth to smaller sized but more numerous dust grains. The observed scattered stellar light arises predominantly not from parent bodies but rather from their dust progeny. Thus the second step of our procedure is to track dust trajectories. We take each parent to release a dust grain with the same instantaneous position and velocity as its parent's. The trajectory of a grain of given β (force of radiation pressure relative to that of stellar gravity; β scales inversely as grain radius) is then integrated forward under the effects of radiation pressure and Poynting-Robertson drag. We carry out integrations for $\beta \in (0, 0.00625, 0.0125, \ldots, 0.4)$. For β approaching the radiation blow-out value of $\sim$1/2, grains execute highly elongated orbits whose periastra are rooted within the birth ring. Integrations last 0.1 Myr, corresponding to the collisional lifetime of grains in Fomalhaut's belt, as estimated from the inferred optical depth of the belt.

Third, we superpose the various β-integrations to construct maps of optical depth normal to the belt plane. To reduce the shot noise associated with a finite number of grains, we smear each grain along its orbit: each grain is replaced by an elliptical wire whose linear density along any segment is proportional to the time a particle in Keplerian motion spends traversing that

segment. We compute the optical depth presented by the collection of wires, weighting each β-integration according to a Dohnanyi (*12*) grain size distribution. This distribution, which reflects a quasi-steady collisional cascade in which parent bodies grind down to grains so small they are expelled by radiation pressure, is assumed to hold in the birth ring, where dust densities are greatest and collision rates highest.

The final step is to compare the optical depth profile of our dynamical model with that of a scattered light model adjusted to fit the 2004 HST image of Fomalhaut's belt (*6*). We focus on the one belt property that seems most diagnostic of planet mass and orbit: the belt's inner edge, having a semimajor axis of $a_{\rm inner} = 133$ AU according to the scattered light model. This edge marks the outer boundary of the planet's chaotic zone (*7*). The chaotic zone is a swath of space enclosing the planet's orbit which is purged of material because of dynamical instabilities caused by overlapping first-order mean-motion resonances (*13*). For a given planet mass M, we adjust the planet's semimajor axis a until the dynamical model's optical depth attains half its maximum value at $a_{\rm inner}$ (Fig. 2, bottom panel). Applying this procedure, we find that

$$a_{\rm inner} - a = 2.0(M/M_*)^{2/7}a \quad (1)$$

where M_* is the central stellar mass. This relation can be used to determine M once a secure value for a is determined by future multi-epoch astrometry.

Two trends that emerge from our modeling imply that the mass of the planet should be low. First, as M increases, the planet more readily perturbs dust grains onto eccentric orbits, and the resultant optical depth profile becomes too broad at distances $\gtrsim$ 140 AU (Fig. 2, bottom panel). Second, to not disrupt the belt, larger mass planets must have smaller orbits, violating our estimate for the current stellocentric distance of Fomalhaut b (Fig. 2, top two panels). Together, these considerations imply that $M < 3M_{\rm J}$, for which the corresponding semimajor axes and eccentricities are $a > 101.5$ AU and $e \approx 0.11$–0.13, respectively. For an intrinsic semimajor

axis of 115 AU for Fomalhaut b, the dynamical model predicts that $M \approx 0.4\ M_{\rm J}$ and $e \approx 0.12$. This last result is similar to that of Quillen (*7*), who predicts an upper mass limit of $\sim 0.3\ M_{\rm J}$ and a semimajor axis of 119 AU. Both models identify the boundary of the planet's chaotic zone with the belt's inner edge. However, the quantitative details of our model are more realistic [see also (*14*)]: the belt as a whole is modeled, not just its inner edge; parent bodies are handled separately from dust grains, and only the latter are used to compare with observations; stellar radiation pressure is accounted for; parent bodies are screened for dynamical stability over the system age; and grain-grain collisions are recognized as destructive, so that dust particle integrations are halted after a collision time.

Model Planet Atmospheres

Comparison between our photometric data and model planet atmosphere spectra indicate that Fomalhaut b may be a cooling Jovian-mass exoplanet with age 100-300 Myr (Fig. 3). A planet atmosphere model with effective temperature $T_{\rm eff}$ = 400 K and radius 1.2 R_J, for which the bolometric luminosity is $3.4 \times 10^{-7}\ L_\odot$ (*15-16*), reproduces the observed 0.8 μm flux. This model implies that the luminosity of Fomalhaut b is lower than any other object observed outside the solar system, and thus that it is not a young brown dwarf or a more massive object. Theoretical cooling tracks of objects with $T_{\rm eff}$= 400 K and ages $>$100 Myr are insensitive to uncertain initial conditions (see figure 1 of *15*). The luminosity on these tracks is given by $L \sim 2 \times 10^{-7} (M/2M_J)^{1.87} (t/200{\rm Myr})^{-1.21} L_\odot$, implying that the mass of Fomalhaut b is 1.7–3.5 M_J. The error in the mass is dominated by the age uncertainty.

Relative to the models of planet atmospheres, the flux of Fomalhaut b is too faint by at least a factor of a few at 1.6 μm, and the upper limit set by observations at 3.8 μm is only marginally consistent with the models. However, the various models disagree with each other by similar factors at 1.6 μm, partly because of theoretical uncertainties associated with the strengths of the

CH_4 vibrational bands. Moreover, our hypothesized effective temperature is near the condensation temperature of water clouds, and such clouds are a large source of uncertainty in planet atmosphere models. Nevertheless, our observations at 1.6 μm and 3.8 μm exclude a warmer (more massive) planet.

Choosing a 400 K, 46 m/s/s, 5$\times$ solar abundance model from (*15*) as a baseline, we can investigate the effects of gravity and composition using theoretical exoplanet model spectra (*15-16*). The elevated abundance set is chosen to be representative of solar system gas giants. The temperature and gravity of this model are a good match to a 200 Myr, 2.5 $M_{\rm J}$ exoplanet. As previously noted, this model accounts for the 0.8 μm flux, but over predicts the 1.6 μm band flux by a factor of three. Cooler models (350 K) cannot simultaneously reproduce the 0.8 μm flux without violating the long wavelength flux limits, while for hotter models (500 K) the 1.6 μm upper limit becomes particularly problematic. If there is a significant thermal photospheric contribution to the 0.8 μm flux, then 400 K is a rough upper limit to the temperature of the object.

The 400 K, solar abundance model has reduced methane opacity which causes it to be unacceptably bright in the H band. The colors and fluxes also depend on the surface gravity. Models from (*15*) for 10 m/s/s and 215 m/s/s are also available: the colors of the low gravity model are too red in both [0.8 μm $-$ 1.6 μm] and [0.8 μm $-$ 3.8 μm] to be acceptable. Thus, if the gravity is lower than our nominal assumption, corresponding to approximately a 0.5 $M_{\rm J}$ object, then we estimate that the upper limit on temperature is raised by about 50 K. The colors of the high-gravity 400 K model are similar to those of the 46 m/s/s one.

Other Sources of Optical Emission

From 0.6 to 0.8 μm, Fomalhaut b is bluer than the models predict (Fig. 3). Furthermore, between 2004 and 2006 Fomalhaut b became fainter by $\sim$0.5 mag at 0.6 μm . Photometric vari-

ability and excess optical emission cannot be explained by exoplanet thermal radiation alone. The 0.6 μm flux might be contaminated by Hα emission (SOM) that is detected from brown dwarfs (*17, 18*). Variable Hα emission might arise from a hot planetary chromosphere heated by vigorous internal convection, or trace hot gas at the inner boundary of a circumplanetary accretion disk, by analogy with magnetospheric emission from accreting T Tauri stars (e.g., *19*). If a circumplanetary disk is extended, the starlight it reflects might contribute to the flux detected at 0.6 and 0.8 μm. To explain our observed fluxes requires a disk radius $\sim 20 - 40$ R_J, comparable to the orbital radii of Jupiter's Galilean satellites (SOM). The need for additional sources of luminosity implies that the mass inferred from the 0.8 μm flux alone is an upper limit.

As remarkably distant as Fomalhaut b is from its star, the planet might have formed *in situ*. The dust belt of Fomalhaut contains at least three Earth masses of solids in its largest collisional parent bodies. Adding enough gas to bring this material to cosmic composition would imply a minimum primordial disk mass of 1 M_J, comparable to the upper mass limit of Fomalhaut b. Alternatively, the planet might have migrated outward by interacting with its parent disk (*20*), or by gravitationally scattering off another planet in the system and having its eccentricity mildly damped by dynamical friction with surrounding disk material (*21*).

References and Notes

1. D. E. Backman, F. C. Gillett, in *Cool Stars, Stellar Systems and the Sun*, eds. J. L Linsky and R.E. Stencel (Springer-Verlag, Berlin), pp. 340-350 (1987).

2. D. Mouillet, J. D. Larwood, J.C.B. Papaloizou, A. M. Lagrange, *Mon. Not. R. Astron. Soc.* **292**, 896 (1997).

3. M.C. Wyatt, *et al. Astrophys. J.* **527**, 918 (1999).

4. 1 pc = 3.09×10^{18} cm

5. K. Stapelfeldt, *et al.*, *Astrophys. J. Suppl. Ser.* **154**, 458 (2004).

6. P. Kalas, J. R. Graham, M. Clampin, *Nature* **435**, 1067 (2005).

7. A. Quillen, *Mon. Not. R. Astron. Soc.* **372**, L14 (2006).

8. D. Barrado y Navascues, *Astron. Astrophys.* **339**, 839 (1998).

9. C. D. Murray, S. F. Dermott, *Solar System Dynamics.* (Cambridge Univ. Press, Cambridge, U.K., 1999).

10. B. Paczynski, *Astrophys. J.* **216**, 822 (1977).

11. L. E. Strubbe, E. I. Chiang, *Astrophys. J.* **648**, 652 (2006).

12. J. W. Dohnanyi, *J. Geophys. Res.* **74**, 2531 (1969).

13. J. Wisdom, *Astron. J.* **85**, 1122 (1980).

14. E. Chiang, E. Kite, P. Kalas, J R. Graham, M. Clampin, *Astrophys. J.*, in press (2008).

15. J.J. Fortney, *et al.*, *Astrophys. J.* **683**, 1104 (2008).

16. A. Burrows, D. Sudarsky, J. I. Lunine, *Astrophys J.* **596**, 587 (2003).

17. A. J. Burgasser, *et al.*, *Astron. J.* **120**, 473 (2000).

18. C. Marois, B. Macintosh, T. Barman, *Astrophys. J.* **654**, L151 (2007).

19. L. Hartmann, R. Hewett, N. Calvet, *Astron. J.* **426**, 669 (1994).

20. D. Veras, P. J. Armitage, *Mon. Not. R. Astron. Soc.* **347**, 613 (2004).

21. E. B. Ford, E. I. Chiang, *Astrophys. J.* **661**, 602 (2007).

22. J. Davis, *et al., Astron. Nachr.* **326**, 25 (2005).

23. P.K. acknowledges support from GO-10598, and K.S. and J.K. acknowledge support from GO-10539, provided by NASA through a grant from STScI under NASA contract NAS5-26555. E.C. acknowledges support from NSF grant AST-0507805. M.F. acknowledges support from the Michelson Fellowship Program, under contract with JPL, funded by NASA. Work at LLNL was performed under the auspices of DOE under contract DE-AC52-07NA27344. E.K. acknowledges support from a Berkeley Fellowship. We thank the staff at STScI, Keck and Gemini for supporting our observations. We are thank Dr. Christian Marois for improving our analysis of Keck data.

Supporting Online Material (SOM)

SOM Text

Fig. S1

Tables S1 to S4

References

Supporting Online Material

Observing Method

Observations with the Hubble Space Telescope (HST) were obtained with the Advanced Camera for Surveys (ACS) High Resolution Channel (HRC) in its coronagraphic mode (*S1*). The HRC is a 1024×1024 pixel CCD with a 1.8″ coronagraphic occulting spot near the center of the detector, and a 3.0″ occulting spot toward the upper left edge. After a correction for geometric distortion the pixel size is 25×25 mas. In 2004 we placed Fomalhaut behind the 1.8″ occulting spot only, whereas in 2006 we imaged Fomalhaut behind both occulting spots (Table S1). Even

though the occulting spots block the core of the stellar point spread function (PSF), a significant halo of light is present in the entire CCD frame. We use two separate strategies to remove this PSF halo: 1) We observe another bright star (Vega) with the coronagraph and use this template PSF to subtract the PSF of Fomalhaut, and (2) We image Fomalhaut such that the detector is rotated at different angles relative to the sky. In the instrument reference frame the PSF is quasi-static, whereas astrophysical features rotate. The 2006 data acquire Fomalhaut at four separate position angles (PA) of the sky on the detector, with a maximum PA separation of 6^{o}. Taking the median value of these frames gives a master PSF that does not contain the astrophysical features. The master PSF is then subtracted from the individual images, which are then rotated to a common orientation and combined. Technique 2 is known in the literature as roll deconvolution or angular difference imaging (ADI; *S2-S4*).

Table S1 catalogs our observations. Fomalhaut b is detected independently in each row with an F606W and F814W observations. For each of these rows, Fomalhaut b is detected using both PSF subtraction techniques outlined above. False-positives are defined as apparent point sources that cannot be consistently confirmed among these data sets.

Table S1: Fomalhaut Observing log

Observatory	Instrument	UT Date	Filter	Exp. Time (s)
HST 2.4-m	ACS/HRC 1.8″ spot	2004 Oct. 25	F606W	1320
	..... 1.8″ spot	2004 Oct. 26	F606W	1320
	..... 1.8″ spot	2006 July 14	F435W	6525
	..... 3.0″ spot	2006 July 15-16	F435W	6525
	..... 1.8″ spot	2006 July 17-19	F606W	7240
	..... 3.0″ spot	2006 July 19-20	F606W	7240
	..... 1.8″ spot	2006 July 18	F814W	5430
	..... 3.0″ spot	2006 July 19	F814W	5430
Keck II 10-m	NIRC2 2.0″ spot	2005 July 17	H	3790
		2005 July 27	H	4320
		2005 July 28	H	4890
		2005 Oct. 21	H	5310
		2005 Oct. 22	CH4	4774
Gemini N 8-m	NIRI	2008 Sep. 17-18	L′	6006

Keck II observations with adaptive optics used the NIRC2 near-infrared camera located at the Nasmyth of the telescope where the sky rotates relative to the instrument focal plane. We used a camera scale of 0.04″ per pixel and a 2.0″ diameter, semi-transparent occulting spot. Though the instrument has reimaging optics to fix the sky angle relative to the detector reference frame, we permit the sky to rotate in order to employ PSF subtraction technique 2 (ADI). Gemini South observations at L′, without adaptive optics correction, were executed in a similar manner to employ the ADI technique. We used the NIRI F/32 camera with 22 mas pixels, giving a $22.4'' \times 22.4''$ field of view. Fomalhaut b is not detected in either the Keck II or Gemini North data.

Astrometry

The astrometric reference frame is established relative to the star Fomalhaut as there are no other adequately bright stars contained within the ACS/HRC field of view. The significant source of astrometric uncertainty is determining the position of Fomalhaut behind the ACS/HRC occulting spots. Successive frames may be registered at the sub-pixel level relative to each other by mutual subtraction, but a fiducial frame is required where the pixel position of Fomalhaut behind the occulting spot is estimated. This is achieved by minimizing the residuals when a frame is subtracted from a copy of itself rotated by 180°. The residuals are minimized when the assumed center of rotation is nearest the position of the star behind the spot. The self-subtraction center positions can be compared to the relative center positions determined by subtracting images of Fomalhaut obtained in successive orbits. We thus estimate the accuracy of determining the location of Fomalhaut behind the occulting spots using 180° self-subtraction technique as $\pm$0.5 pixel (12.5 mas, or 0.10 AU at the distance to Fomalhaut). This value is an upper limit to the possible difference between the true and estimated positions of Fomalhaut.

The centroid position of Fomalhaut b were measured in three versions of the final F606W

processed images in 2004, and seven versions from the 2006 F606W processed data. All images were rotated to the orientation shown in Fig. 1. We find a standard error of 0.31 and 0.55 pixel along the x and y directions in the 2004 data. In the 2006 measurements the corresponding standard errors are 0.09 and 0.32 pixel. Adding these uncertainties in quadrature to the uncertainties in the position of Fomalhaut at each epoch gives 0.87 pixel for the 1-σ uncertainty in the estimated motion of Fomalhaut b between epochs. This translates to 0.022 arcsecond or 0.169 AU.

The fact that Fomalhaut b is orbiting Fomalhaut is robust because the apparent orbital motion of 7.3 pixels between epochs is significantly greater than these uncertainties, as well as the PSF full-width at half-maximum of $\sim$2.7 pixels. Fomalhaut b cannot be a background objects as shown in Fig. S1. The empirical RMS accuracy in the position angle achieved in ACS data is 0.003 degrees (*S5*), which corresponds to an insignificant uncertainty of 0.03 pixel at the radial position of Fomalhaut b.

Photometry

In the cases where Fomalhaut b was detected (HST), we report photometry corrected to an infinite aperture using DAOPHOT and an empirical curve of growth derived from the data (Table S2). Zeropoints for the HST data are obtained from (*S6*). The error bars quoted are statistical only. The standard error derived from multiple versions of the F606W data with different PSF subtraction techniques is 0.10 mag and 0.05 mag for the 2004 and 2006 data, respectively.

Table S2: Photometry on Fomalhaut b

UT Date	Filter	λ_c (μm)	Magnitude	Error (mag)	Detection?
2004-10-25	F606W	0.606	24.43	0.08	Yes
2004-10-26	...	...	24.29	0.09	Yes
2005-07-21	H	1.633	$>$22.9	3σ limit	No
2005-10-21	CH_4S	1.592	$>$20.6	3σ limit	No
2006-07-14/20	F606W	0.606	25.13	0.09	Yes
...	F814W	0.814	24.55	0.13	Yes
...	F435W	0.435	$>$24.7	3σ limit	No
2008-09-17/18	L$'$	3.78	$>$16.6	3σ limit	No

Photometric calibration of the Keck upper limits is a multi-step process. Data were scaled to a common signal level using background star observations prior to combination. For the multi-night combination of H-band data, we use the July 17 observations for photometric calibration because of that night's exceptional conditions. The peak brightness of Fomalhaut was measured through the partially transmissive occulting spot in short exposure images. These measurements were used to determine an on-axis sensitivity calibration using the 2MASS photometry of Fomalhaut and the previously measured occulting spot transmission. We derived a sensitivity curve by measuring the standard deviation of fluxes in apertures of 3 pixel diameter and measured the value at the predicted angular separation of Fomalhaut b. Finally, we noted that the Strehl ratio at the location of Fomalhaut b is degraded due to anisoplanatism. We estimated a decrease in sensitivity of 0.75 mag, which corresponds to an isoplanatic angle of 13$''$ at 1.6 μm.

Calibration of the Gemini L'-band data was performed using observations of a standard star, HR 9016A, which were obtained in the middle of the observing sequence each night. The unsaturated exposures of the standard were used to derive a photometric zero point and aperture correction for each night. The data from the different nights were scaled to the same throughput in apertures of 0.3$''$ diameter prior to combination. The upper limit to Fomalhaut b was obtained by measuring the standard deviation of flux in 0.3$''$ apertures in an arc along $\pm$45 degrees of

the predicted position of Fomalhaut b. We adopt a factor of 2 in decreased sensitivity due to the estimated Strehl degradation from errors in centroiding the saturated images of Fomalhaut.

Bolometric luminosity

In this section and following, we consider various possibilities for the origin of the detected optical flux. Here, we assume that the F814W flux is pure thermal emission from the planet, which consistent with the model atmosphere from (*S7*) where $T_{eff} = 400$ K; g = 46 m s^{-2}; and 5$\times$ solar metallicity. With this effective temperature, and with a planet radius 1.2 R_J, the bolometric flux at Earth is:

$$F = \left(\frac{r_p}{d_p}\right)^2 \sigma_{SB}\, T_{eff}^4 = 1.86 \times 10^{-13}\ \mathrm{erg\ s^{-1}\ cm^{-2}} \quad (2)$$

where r_p is the the radius of Fomalhaut b, d_p is the heliocentric distance, and σ_{SB} is the Stefan-Boltzmann constant. As a check, we integrate the flux from the (*S7*) high resolution model spectrum, and obtain:

$$\int_{6.0\times10^{12}\ \mathrm{Hz}}^{7.5\times10^{14}\ \mathrm{Hz}} F_\nu\, d\nu = 1.80 \times 10^{-13}\mathrm{erg\ s^{-1}\ cm^{-2}} \quad (3)$$

The smaller value is expected because the model is tabulated over a finite frequency range and some power is missing in the numerical integration. The corresponding luminosity is $\sim 3\times10^{-7}$ L$_\odot$, which indicates that Fomalhaut b is the faintest known object outside of the solar system.

Hα Emission

Photometry in the F606W filter varies between 25.1 and 24.3 mag (0.36 and 0.75 μJy, respectively). Assuming that the flux is due to a single, narrow emission line, the equivalent line flux would be $\Delta\nu F_\nu = 0.7 - 1.5 \times 10^{-14}\ \mathrm{erg\ s^{-1}\ cm^{-2}}$. The fractional luminosity would be $L_{\mathrm{H}_\alpha}/L_{\mathrm{bol}} = 0.4 - 0.8\%$. The H$\alpha$ emission from Fomalhaut b would be similar to that suggested for GQ Lup b, where $L_{\mathrm{H}_\alpha}/L_{\mathrm{bol}} = 2\%$ (*S8*).

The Hα emission hypothesis can be tested with an optical spectrum of Fomalhaut b. If confirmed, then a key problem is explaining the origin of gas around a 200 Myr yr old star (two orders of magnitude older than GQ Lub b). Equating the Hα luminosity to accretion luminosity, the accretion rate is 10^{-11} M_J yr^{-1}, or 0.002 M_J over the age of the system (assuming 100% efficiency). If we assume that the efficiency is $\sim$1%, then the total gas accretion is 0.2 M_J.

Dust Cloud Model

We explore the possibility that Fomalhaut b represents reflected light from an unresolved dust cloud that is not gravitationally bound and therefore not associated with a planet. In this scenario the cloud arises from the stochastic, catastrophic collision of two parent bodies analogous to Kuiper Belt Objects or short-period comets in the solar system. The event is improbable at the location of Fomalhaut b compared to regions closer to the star where the collision timescales are significantly shorter, or farther from the star where the number density of parent bodies is enhanced in order to replenish the visible belt with fresh dust.

Since Fomalhaut b appears as a point source in the HST data, the maximum size of the dust cloud corresponds to the full-width at half-maximum of the PSF, which is 69$\pm$6 mas or 0.53 $\pm$0.05 AU (compared against the background star shown in Fig. S1, which has FWHM = 68 $\pm$ 4 mas). A dust cloud could originate from a catastrophic collision between two planetesimals, but the event must be recent because even in the absence of stellar radiation pressure and Poynting-Robertson drag, the different orbital period of a dust grain located at the inner boundary of the cloud (i.e. closest to Fomalhaut) versus the outer boundary of the cloud would shear the cloud into an arc, ultimately becoming a ring of material orbiting Fomalhaut.

The dust cloud will contain a size distribution of grains, though the scattered light images are predominantly sensitive to grain sizes with $x = 2\pi a/\lambda \sim 1$, where a is the grain radius. In our model of a dust cloud we assume a size distribution with $a_{min} < a < a_{max}$ following a dif-

ferential size distribution $dn/da = n_o(a/a_o)^{-3.5}$. We note that due to radiation pressure from Fomalhaut, grains smaller than 3−8 μm (depending on porosity) are ejected from the system on free-fall timescales (*S9*). We therefore use Mie theory to calculate the apparent magnitude and scattered light color of a dust cloud with a_{min} = 0.01 μm and a_{max} = 1000 μm ($m^{0.01}$ in Table S3) and a_{min} = 8 μm and a_{max} = 1000 μm (m^{8} in Table S3). These values represent two extremes of a fresh dust cloud with small grains still present within the cloud, and a later epoch where only grains larger than the radiation pressure blowout size of ∼8 μm have survived. We test grains composed of water ice (density = 1.0 g cm^{-3}; $m_{\rm ice}$ in Table S3) and refractory carbonaceous material (density = 2.2 g cm^{-3}; *S10*; $m_{\rm LG}$ in Table S3). The results for these two calculations are given in Table S3. The total grain mass (and hence the total scattering surface area) is adjusted such that the integrated light in F814W from the model matches the observations. In the case of $m^{8}_{\rm ice}$, the total mass is 1.24×10^{21} g, which corresponds to the disruption of a 67 km water ice body. However, the total grain mass depends strongly on the value selected for a_{max}. Perhaps a more useful calculation is the minimum grain mass assuming the grain size distribution is nearly monodisperse and peaks where the scattering efficiency is highest. For these optical observations, the scattering efficiency is highest for grains $0.1 - 0.2$ μm in size, giving a minimum dust mass in the cloud $M_d = 4.1 \times 10^{18}$ $(\rho_g/1.0$ g cm$^{-3})$ g. Therefore, for water ice, the minimum grain mass is 4.1×10^{18} g, corresponding to the disruption of a 10 km radius object.

Table S3: Dust cloud model for Fomalhaut b

Filter	$m_\star$	$m_{\rm Fom-b}$	$m^{0.01}_{\rm ice}$	$m^{0.01}_{\rm LG}$	$m^{8}_{\rm ice}$	$m^{8}_{\rm LG}$
F435W	1.25	>24.7 3-σ	24.37	24.59	24.50	24.83
F606W	1.16	25.13 ± 0.09	24.46	24.57	24.67	24.68
F814W	1.08	24.55 ± 0.13	24.55	24.55	24.55	24.55

Table S4: Colors of the dust cloud model

Filter	$\Delta m_\star$	$\Delta m_{\rm Fom-b}$	$\Delta m_{\rm ice}^{0.01}$	$\Delta m_{\rm LG}^{0.01}$	$\Delta m_{\rm ice}^{8}$	$\Delta m_{\rm LG}^{8}$
F435W - F606W	0.09	$<$0.43	-0.09	0.02	-0.17	0.15
F606W - F814W	0.08	0.58	-0.09	0.02	0.12	0.13

In Table S4 we give the apparent optical colors. The dust cloud model explains the Fomalhaut b observations with respect to the non-detections in H and L'. Otherwise, the dust cloud model is inconsistent with the Fomalhaut b photometry because: (1) A dust cloud should have been detected in the F435W data (except in the case of $m_{\rm LG}^{8}$ in Table S4), and (2) The color of a dust cloud is significantly bluer than the observed red color of Fomalhaut b (Table S3). A third significant problem with the dust cloud model is explaining the F606W variability observed over two epochs. The cumulative scattering surface area would have to drop by 63% over 1.73 year to account for the 0.5 mag decrease in optical magnitude. One possible mechanism is that the 2004 data show Fomalhaut b with a small grain component, but in 2006 the small grains have dispersed due to radiation pressure. Removing all grains < 8 μm in size from the first model without renormalizing the F814W flux results in a brightness decrease of 2.23 mag in F606W. Thus an 0.5 mag decrease is possible by tuning the removal of small grains over 1.73 years. This scenario demands that we have observed the cloud at a fortuitous time right after it has been produced, but before all of the small grains are blown out.

Taking all four arguments together – the low probability of the stochastic collision at the position of Fomalhaut b, the fortuitous timing to explain variability, the non detection in the F435W filter, and the somewhat discrepant observed optical colors compared to a model – the dust cloud hypothesis appears inadequate to explain the observed properties of Fomalhaut b.

Reflected light from a planet surrounded by an extended dust disk

We consider the hypothesis that the Fomalhaut b observations are explained by reflected

light from a Jovian planet surrounded by a large ring system. First, we consider reflected light from the planet alone. The flux received at Earth from the star (Fomalhaut) is:

$$f_\star = \frac{L_\star}{4\pi\ D^2} = \frac{6.34 \times 10^{27}}{4\pi\ (2.379 \times 10^{17})^2} = 8.914 \times 10^{-9}\ \mathrm{Wm}^{-2} \tag{4}$$

where $L_\star$ is the stellar luminosity in watts (W; *S12*), and D is the heliocentric distance (7.688 pc = 2.379×10^{17} m). The stellar flux received by a planet at d=115 AU radius from Fomalhaut is:

$$f_o = \frac{L_\star}{4\pi\ d^2} = \frac{6.34 \times 10^{27}}{4\pi\ (115 \times 1.5 \times 10^{11})^2} = 1.70\ \mathrm{Wm}^{-2} \tag{5}$$

The flux received at earth:

$$f_p = \frac{f_o}{4\pi\ D^2} = \frac{\sigma_p Q_s \times 1.70\ \mathrm{Wm}^{-2}}{4\pi\ (2.379 \times 10^{17})^2} = \sigma_p Q_s \times 2.390 \times 10^{-36}\ \mathrm{Wm}^{-2} \tag{6}$$

where σ_p [m^2] is the projected geometric surface area of the planet and Q_s is the scattering efficiency, such as the product of the geometric albedo and the scattering phase function at the observed phase. It is useful to consider these values as a relative contrast in apparent magnitude:

$$\Delta m = m_p - m_\star = -2.5 \log\left(\frac{f_p}{f_\star}\right) = -2.5 \log\left(\frac{\sigma_p Q_s \times 2.39 \times 10^{-36}}{8.91 \times 10^{-9}}\right) = -2.5 \log(\sigma_p Q_s) + 69 \tag{7}$$

The V band (F606W) apparent magnitude of Fomalhaut is m_V = 1.2 mag, giving $m_p = -2.5\ \log(\sigma_p Q_s)$ + 70.2. If we ignore the reduction in brightness due to viewing phase, the geometric cross section of a 1.2 R_J planet is $\sigma_p = \pi \times (1.2 \times 7.15 \times 10^7 \mathrm{m})^2 = 2.31 \times 10^{16}$ m^2. For $Q_s = 0.5$, the apparent magnitude of this planet m_p = 30.0 mag. Thus, the observed apparent magnitude of Fomalhaut b at optical wavelengths (Table S2) is ∼5 mag brighter than light reflected from a Jupiter.

Now we consider that the planet is surrounded by dust grains analogous to circumplanetary rings. Since this is a flattened disk, the geometric cross section scales as cos(i), where i is the inclination to the line of sight ($i = 0^{\rm o}$ is a face-on orientation). Consider that the main, optically thick rings of Saturn extend out to Saturn's Roche radius, or about 2 planetary radii. If Fomalhaut b also harbored a ring system extending to its Roche radius, then σ_p would be replaced by the ring cross section $\sigma_{pr} \sim \sigma_p \times 2^2 \times \cos(66^o) \sim 1.6\sigma_p$. Assuming again Q_s = 0.5, the apparent magnitude of the system would be m_{pr} = 29.5 mag, or about 4.5 mag too faint compared to what is actually observed.

To make up for this shortcoming, the scattering surface area of the planet+ring system would have to increase by yet another factor of $\sim$60. This would correspond to about $\sim$16 planetary radii. If the effective albedo of the ring particles is closer to 0.1—and in fact outer solar system albedoes are typically this low—then the rings must extend to $\sim$35 planetary radii. An optically thick ring system that is 16–35 planetary radii large is better described as a protosatellite, circumplanetary disk. For example, the outermost Galilean satellite of Jupiter, Callisto, has a planetocentric distance of about $\sim$27 Jupiter radii. Regular satellites have prograde motion that indicates formation $in\ situ$ around the planet.

Though in some respects this is similar to the pure dust cloud model, the planet+disk hypothesis has several advantages: (1) The presence of a planet allows for a wider range of physical phenomena to account for the F606W variability, such as the Hα hypothesis. (2) The location of Fomalhaut b just inside the dust belt is consistent with the predicted location of a planet gravitationally sculpting the belt's inner edge. (3) The existence of a planet permits a system of dust to be spatially confined rather than dispersed due to shearing or radiation pressure.

SOM References

1. H. C. Ford, *et al.*, *S.P.I.E.* **4584**, 81 (2003).

2. C. Marois, *et al., Astrophys. J.* **641**, 556 (2006).

3. M. P. Fitzgerald, P.G. Kalas, G. Duchene, C. Pinte, & J.R. Graham *et al., Astrophys. J.* **670**, 536 (2007).

4. D. Lafrenière *et al., Astrophys. J.* **670**, 1367 (2007).

5. R. P. van der Marel, J. Anderson, C. Cox, V. Kozhurina-Platais, M. Lallo, E. Nelan, Instrument Science Report ACS 2007-007 (Space Telescope Science Institute; Baltimore), (2007).

6. Sirianni, M., *et al., PASP* **117**, 1049 (2005).

7. J.J. Fortney, *et al., Astrophys. J.* **683**, 1104 (2008).

8. C. Marois, B. Macintosh, T. Barman, *Astrophys. J.* **654**, L151 (2007).

9. P. Artymowicz & M. Clampin *Astrophys. J.* **490**, 863 (1997).

10. A. Li, J. M. Greenberg, *Astron. Astrophys* **323**, 566 (1997).

11. J. Davis, *et al., Astron. Nachr.* **326**, 25 (2005).

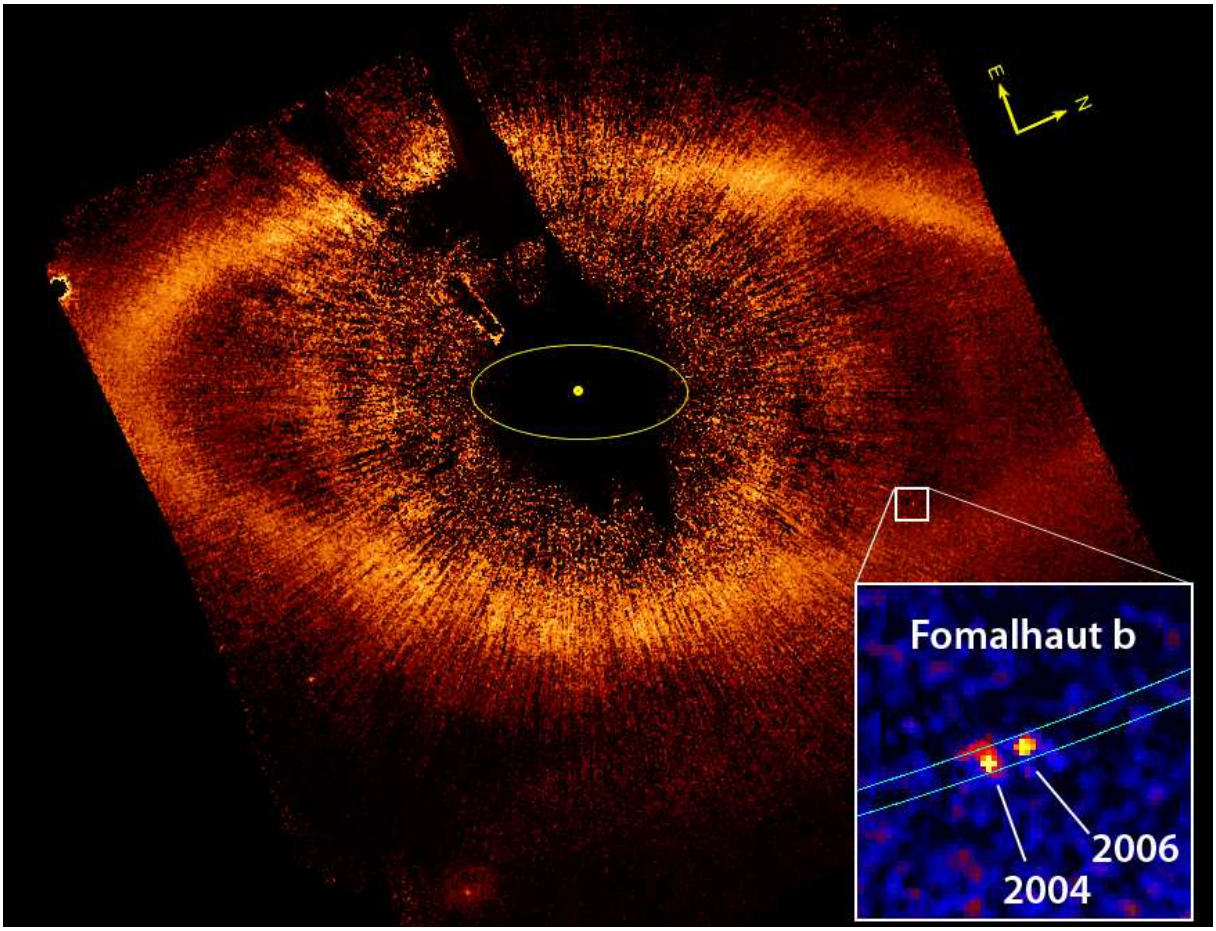

Figure 1: HST coronagraphic image of Fomalhaut at 0.6 μm showing the location of Fomalhaut b (white square) 12.7″ radius from the star and just within the inner boundary of the dust belt. All the other apparent objects in the field are either background stars and galaxies or false-positives. The fainter lower half of the dust belt lies behind the sky plane. To obtain an orientation with north up and east left, this figure should be rotated 66.0° counterclockwise. The yellow circle marks the location of the star behind the occulting spot. The yellow ellipse has a semimajor axis of 30 AU at Fomalhaut (3.9″) that corresponds to the orbit of Neptune in our solar system. The inset is a composite image showing the location of Fomalhaut b in 2004 and 2006 relative to Fomalhaut. Bounding Fomalhaut b are two elliptical annuli that are identical to those shown for Fomalhaut's dust belt (*6*), except that here the inner and outer annuli have semimajor axes of 114.2 and 115.9 AU, respectively. The motion of Fomalhaut b therefore appears to be nested within the dust belt.

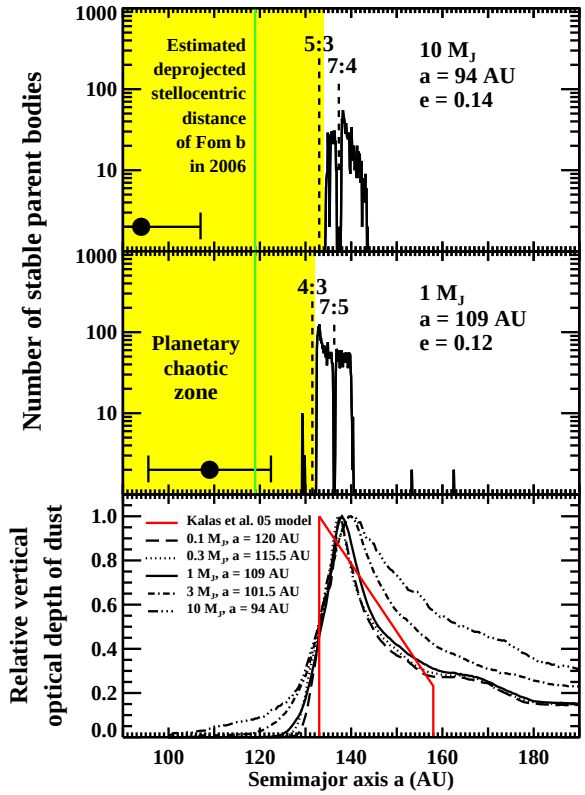

Figure 2: Dynamical models of how Fomalhaut b gravitationally sculpts the belt [see also (*14*)]. *Top two panels*: Histograms of time-averaged semimajor axes of parent bodies that survive 100-Myr-long integrations with Fomalhaut b, whose parameters are chosen to reproduce the belt's inner edge at 133 AU and ellipticity of 0.11. Parent bodies are evacuated from Fomalhaut b's chaotic zone (yellow region). Gaps open at the planet's resonances, akin to the solar system's Kirkwood gaps. Black circles and bars mark the range of stellocentric distances spanned by the model orbits for Fomalhaut b. The apocentric distance for $10\ M_{\rm J}$ is inconsistent with the observed stellocentric distance of Fomalhaut b (green line). The $1\ M_{\rm J}$ model is consistent. *Bottom panel*: Vertical optical depth profiles of dust generated from parent bodies. The planet orbit is tuned so that the optical depth is at half maximum at 133 AU, the location of the inner edge of the scattered light model from (*6*) (red curve), which itself is an idealized and non-unique fit to the HST data. While the dynamical and scattered light models do not agree perfectly, lower planet masses are still inferred because they do not produce broad tails of emission at $a \gtrsim 140$ AU. At $a \gtrsim 160$ AU, the HST data are too uncertain to constrain any model.

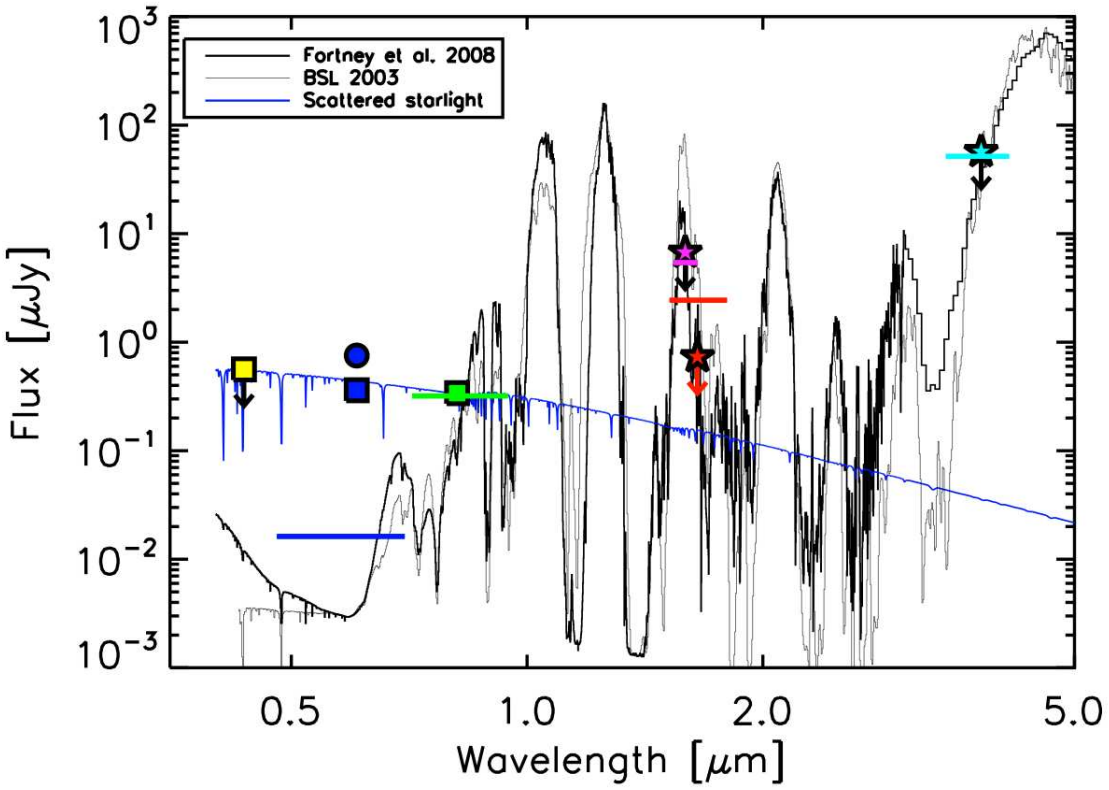

Figure 3: Photometry on Fomalhaut b shows the F435W 3-σ upper limit (yellow square), two F606W measurements (blue square=2006, blue circle=2004), the F814W photometry (green square), 3-σ upper limits for Keck observations in the CH_4 passband (purple solid star) and the H band (red solid star), and a 3-σ upper limits for Gemini observations at L$'$ (light blue star). This is a log-log plot. If we first assume that the F606W variability is due to Hα emission and the F814W detection is due to planet thermal emission, we then proceed to fit a planet atmosphere model from (*15*) to the F814W flux. The heavy solid line represents that planet atmosphere model smoothed to R=1200 with planet radius 1.2 R_J, gravity 46 m s^{-2}, and T=400K (roughly 1-3 M_J at 200 Myr). The horizontal colored lines mark the equivalent broad-band flux found by integrating the model spectrum over the instrumental passband. Other models from (*16*) give a similar spectrum (light solid line), though a factor of 3 - 4 brighter in CH_4 and H band. The model predicts that the planet candidate should have been detected with Keck in the H band, though this prediction is only a factor of a few above our limit. The discrepancy could arise from uncertainties in the model atmosphere (which has never been tested against observation), or from the possibility that the F606W and F814W detections include stellar light reflected from a circumplanetary dust disk or ring system. The solid blue line intersecting the optical data represents light reflected from a circumplanetary disk with radius 20 R_J, a constant albedo of 0.4, and with stellar properties adopted from (*22*).

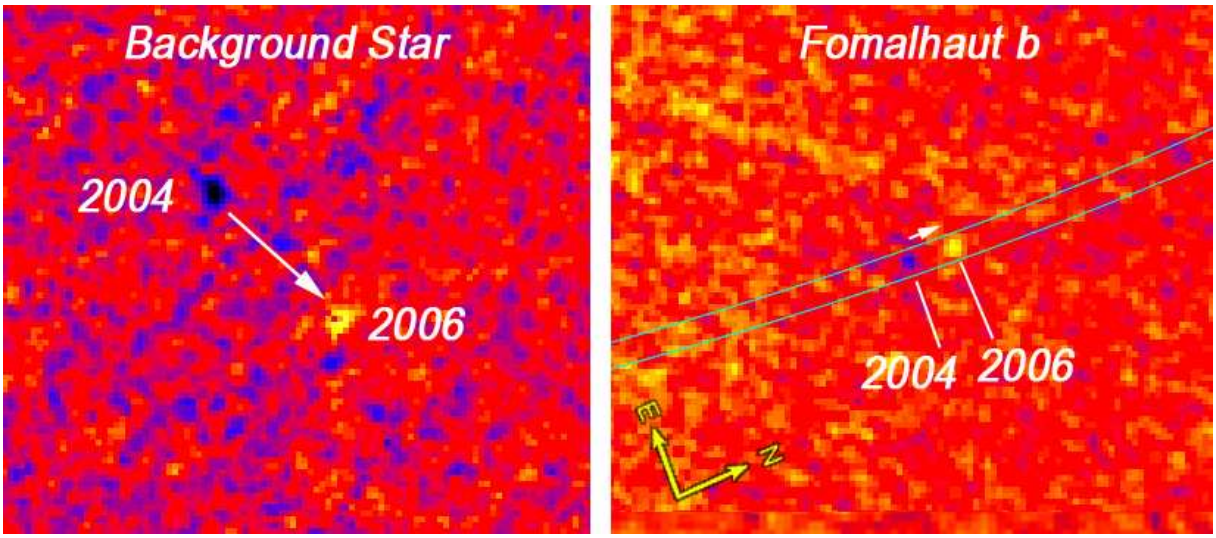

Figure 4: **Fig. S1**: Two enlarged sub-regions (at the same scale) from Figure 1 centered on Fomalhaut b and a background star (located at the 8 o'clock position relative to Fomalhaut in Fig. 1, just outside the dust belt). We show relative motion by registering the 2004 and 2006 data to Fomalhaut and producing the difference image. Background objects are easily distinguished from the planet candidate in terms of the magnitude (0.7 arcsecond) and direction of their motion. In 2004, Fomalhaut b is detected at separation $\rho = 12.61''$ and position angle, PA = 316.86^{o} relative to Fomalhaut. In 2006, Fomalhaut b is at $\rho = 12.72''$ and position angle, PA = 317.49^{o} (recall that the orientation shown here is rotated 66.0^{o} clockwise from one that gives north up and east left).